Surface-Enhanced Infrared Absorption

Masatoshi Osawa

Catalysis Research Center, Hokkaido University
Sapporo 060-0811, Japan
osawam@cat.hokudai.ac.jp

Abstract. Molecules adsorbed on metal island films or particles exhibit 10–1000 times more intense infrared absorption than would be expected from conventional measurements without the metal. This effect is referred to as surface-enhanced infrared absorption (SEIRA) to emphasize the similarities with surface-enhanced Raman scattering (SERS). The electromagnetic interactions of the incident photon field with the metal and molecules play predominant roles in this effect. The chemical interactions of the molecules with the surface can give additional enhancement. The enhancement mechanisms and some applications of SEIRA.

1 Introduction

The optical properties of molecules are dramatically changed when they are adsorbed on rough metal surfaces, metal island films, or metal particles. The best-known example is surface-enhanced Raman scattering (SERS), in which the Raman scattering of molecules is enhanced by millions of times compared with free molecules [1,2,3,4]. A quite similar effect occurs in the mid-infrared region: molecules on metal surfaces show infrared absorption 10–1000 times more intense than would be expected from conventional measurements without the metal [5,6,7,8]. This effect is referred to as surface-enhanced infrared absorption (SEIRA) to emphasize the analogy to SERS.

Since the discovery of this effect in 1980 [5], a number of SEIRA spectra have been observed on various metals. The SEIRA effect is characterized as follows:

1. Enhanced spectra can be observed in the transmission [9,10], attenuated-total-reflection (ATR) [5,6,7], external-reflection [11], and diffuse-reflection modes [12]. In ATR and external-reflection measurements, the observed band intensities depend on the polarization and angle of incidence of the infrared radiation [11,13,14].
2. The enhancement depends greatly on the morphology of the metal surface [15]. Vacuum-evaporated [5,6,7] and electrochemically deposited [16,17,18,19] metal island films, and metal colloids [20,21] are good enhancers. In the case of island films, the largest enhancement is observed when the islands are densely crowded but not touching each other.
3. Both physisorbed and chemisorbed molecules exhibit enhancement. In general, chemisorbed molecules show a larger enhancement than physisorbed molecules.

S. Kawata (Ed.): Near-Field Optics and Surface Plasmon Polaritons,
Topics Appl. Phys. **81**, 163–187 (2001)

4. The enhancement is significant for the first monolayer directly attached to the surface and decays sharply within about 5 nm from the surface [10,22,23,24,25].
5. Vibrational modes that have dipole moment derivative components perpendicular to the surface are preferentially enhanced [26]. This surface selection rule is the same as that in the so-called infrared reflection absorption spectroscopy [27]. The molecular orientation can be determined by using the surface selection rule [28,29,30].
6. Metal island films that exhibit SEIRA have a very broad absorption extending from the visible to the mid-infrared, on which the enhanced absorption bands of the adsorbed molecules are superposed [10]. There exists a linear relationship between the absorption of the metal and the enhancement [10,15].

At least two different mechanisms, the electromagnetic (EM) and chemical mechanisms, are supposed to contribute to the total enhancement [10,31,32] as in the case of SERS [1,2,3,4]. The infrared absorption (A) may be written as

$$A \propto |\partial \boldsymbol{\mu}/\partial Q \cdot \boldsymbol{E}|^2 = |\partial \boldsymbol{\mu}/\partial Q|^2 |\boldsymbol{E}|^2 \cos^2 \theta \tag{1}$$

where $\partial \boldsymbol{\mu}/\partial Q$ is the derivative of the dipole moment with respect to a normal coordinate Q, $\boldsymbol{E}$ is the electric field that excites the molecule, and θ is the angle between $\partial \boldsymbol{\mu}/\partial Q$ and $\boldsymbol{E}$. It should be noted that the intensity of the electric field $|\boldsymbol{E}|^2$ at the surface is not the same as that of the incident photon field: a coupling of the incident photon field to the metal surface can enhance the field [1,2,3,4,33,34]. The EM mechanism assumes an increase of the local electric field at the surface [8,26,35]. The experimental evidence that the enhancement extends to several monolayers away from the surface provides a strong argument that a relatively short-ranged enhanced EM field (i.e. the near field) contributes to the SEIRA effect. On the other hand, the chemical mechanism assumes an increase of $|\partial \boldsymbol{\mu}/\partial Q|^2$ (i.e. the absorption coefficient) due to chemical interactions between the molecule and the metal surface. For example, CO chemisorbed on metal surfaces has an absorption coefficient 2–6 times larger than condensed CO (i.e. overlayers) [36,37,38]. Adsorbed molecules are often oriented in a specific direction with respect to the surface. Since the space average of $\cos^2 \theta$ is 1/3 for randomly oriented molecules, the orientation effect gives an additional enhancement by a factor of three at maximum for vibrational modes that have dipole changes parallel to $\boldsymbol{E}$.

SEIRA spectroscopy (SEIRAS) is now appearing with a wide range of applications. Infrared spectroscopy has been established as a routine molecule-specific technique for qualitative and quantitative purposes. However, the relatively low absorption coefficients of molecules in the infrared region limit its use in many applications. Therefore, SEIRAS techniques that lower the detection limit of infrared spectroscopy are of great interest. Trace amount of molecules, ranging from picograms to nanograms [9,39,40], and very

thin organic and bioorganic films, including Langmuir–Blodgett films and self-assembled monolayers (SAMs) [22,41,42,43,44,45] have been analyzed. SEIRAS can also be used for chemical sensing [18,45,46,47,48]. Since fine metal particles have high catalytic activity in many reactions, SEIRAS is very promising for catalysis research [16,17,19,49,50,51]. Surfaces of nonmetallic materials, such as polymers, semiconductors, glass, human skin, and agricultural products, can also be analyzed by this technique [11,52,53]. Among several applications, great success has been achieved in its application to dynamic studies of electrochemical interfaces [8,25,54,55,56,57,58].

2 Enhancement Mechanisms

2.1 Electromagnetic Mechanism

Vacuum-evaporated thin metal films are used most frequently for SEIRA experiments. Thin metal films that show strong SEIRA are not continuous but consist of metal islands smaller than the wavelength of light, as shown in Fig. 1. The sample shown here is a 10 nm thick (in mass thickness) Ag film on Si. The average dimension of the islands is about 30 nm. If the islands are modeled by ellipsoids of rotation, the aspect ratio of the islands (the ratio of the major to the minor diameter) ranges from 3 to 5. The density, shape, and size of the islands depend on the mass thickness, the evaporation conditions, and the chemical nature of the substrate [15]. As the mass thickness increases, the islands grow in size, contact each other, and eventually form a continuous film. Connection of the islands significantly reduces the enhancement, suggesting that the small metal islands play an important role in the enhancement.

The metal islands are polarized by the incident photon field through the excitation of collective electron resonance, or localized plasmon, modes, and the dipole p induced in an island generates a local EM field stronger than the incident photon field around the island [2,3,33,34], as illustrated in Fig. 2. A detailed theoretical treatment of the local EM field has been given in [33]. It

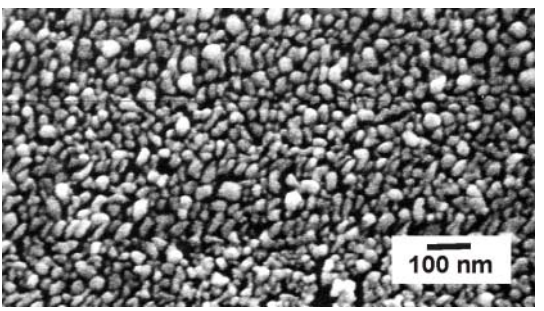

Fig. 1. SEM image of a 10 nm thick Ag film vacuum-evaporated on Si

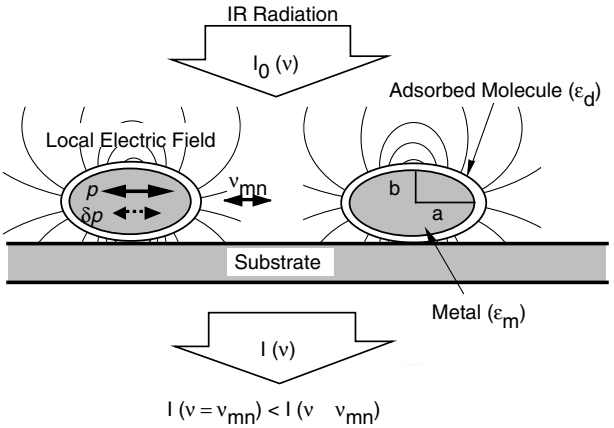

Fig. 2. Schematic representation of the electromagnetic mechanism of SEIRA on metal island films. See text for details. In simulations, the island film is modeled as a set of ellipsoids of rotation with a dielectric function ε_{m}, and the adsorbed molecules are modeled by a thin layer with a dielectric function ε_{d} covering the ellipsoids. The aspect ratio of the ellipsoids is defined as $\eta = a/b$

has been well established that the enhanced EM field strongly enhances the Raman scattering of adsorbed molecules. Figure 3 shows a set of transmission spectra of vacuum-evaporated Ag films on CaF_2 [10]. The strong band around 500 nm is attributed to the collective electron resonances of isolated Ag particles. As the mass thickness increases, the absorption band shifts to longer wavelengths and becomes broader owing to the dipole coupling between islands [59]. It is noteworthy that the tail of this absorption extends

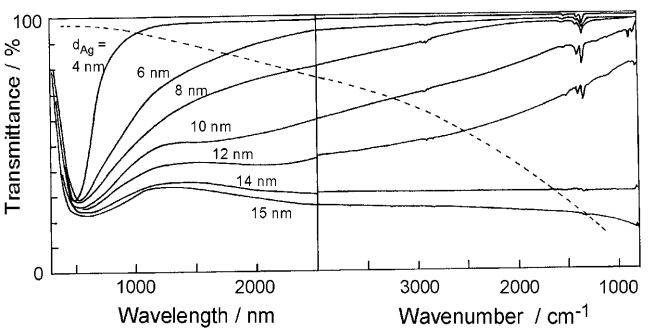

Fig. 3. Transmission spectra of Ag island films evaporated on CaF_2. The mass thickness of each film is shown in the figure. The peaks in the mid-infrared region are of p-nitrobenzoate adsorbed on the island films. The *dashed trace* is the spectrum of a 10 nm thick Ag film calculated from the Fresnel formula and the dielectric function of bulk Ag under the assumption that the film is continuous

well into the mid-infrared region. The observed spectra are very different from the spectrum shown by the dashed line, which was calculated using the dielectric function of bulk Ag and the Fresnel formula [60] under the assumption that the film is continuous. This result suggests that the collective electron resonance is excited even in the mid-infrared region and that the enhanced EM field enhances the infrared absorption of adsorbed molecules. A contribution of such EM effect to SEIRA was suggested also by the linear relationship between the enhanced band intensity and the average EM field intensity within the metal film [13,14].

The intensity of the enhanced EM field decays sharply as the distance from the surface (d) increases, as represented by the following equation [33,61]:

$$|E_{\text{local}}|^2 \propto \left(\frac{a}{a+b}\right)^6, \tag{2}$$

where a is the local radius of curvature of the island. In addition, the local EM field is essentially polarized along the surface normal at every point on the surface of the islands [34] (Fig. 2). Therefore, this model is quite convenient for explaining the relatively short-ranged enhancement and the surface selection rule. However, the EM field enhancement theoretically estimated is only ten-fold or less in the mid-infrared region [10,43] owing to the large imaginary part of the dielectric constants of metals (i.e. the strong damping of localized plasmon modes). Therefore, the total enhancement of up to 1000 cannot be explained by this field enhancement only.

In the case of SERS on island films, the Raman-scattered light polarizes the metal islands and strong Raman scattered light is emitted from the dipoles induced in the metal islands [1,2,3,4,33]. A similar situation may be considered in SEIRA; that is, adsorbed molecules induce additional dipoles δP in the metal islands and perturbe the optical properties of the metal. Since the perturbation is larger at vibrational frequencies of the molecule than at other frequencies, the spectrum of the metal island film should be nearly identical to the spectrum of the molecule. The absorption coefficients of metal islands are smaller than those of the corresponding bulk metals in the infrared region, as revealed by infrared spectroscopic ellipsometric measurements [62], but are still larger than those of molecules. In addition, the volume of the metal in the island film is much larger than that of a monolayer adsorbate. Consequently, the vibrational spectrum of the adsorbate will be observed much more strongly than would be expected from conventional measurements without the metal. That is, a metal island is believed to function as an amplifier in SEIRA. The linear relationship between the band intensity of the adsorbed molecule and the background absorption of the metal can be understood with this assumption.

If the system is assumed to be a continuous composite film consisting of metal particles, adsorbed molecules, and voids (or host medium), the transmittance or reflectance of the composite film can be calculated easily by

using the Fresnel equations [60]. The effective (i.e. space-averaged) dielectric function of the composite film can be connected with the polarization susceptibility (α) of the metal islands by using an effective-medium approximation (EMA) [63]. For the sake of simplicity, a metal island film is modeled as a set of ellipsoids of rotation with a uniform size, as shown in Fig. 2. The rotation axis is perpendicular to the surface. The molecules are assumed to cover the ellipsoid surfaces uniformly.

Among several models, the EMAs proposed by *Maxwell-Garnett* (MG) [64] and *Bruggemann* (BR) [65] are the best known. In the MG model, the effective dielectric function, $\varepsilon_{\mathrm{MG}}$, is connected with α by the following equation [63].

$$\varepsilon_{\mathrm{MG}} = \varepsilon_{\mathrm{h}} \left(\frac{3 + 2F\alpha}{3 - F\alpha} \right) , \tag{3}$$

where F is the filling factor of the metal within the composite layer and ε_{h} is the dielectric constant of the surrounding host medium. The value of α for an ellipsoid coated with molecules can be expressed as a function of the dielectric functions of the bulk metal (ε_{m}), the adsorbed molecule (ε_{d}), and the host as follows [66]:

$$\alpha_{\parallel,\perp} = \left\{ \frac{x}{y} \right\}_{\parallel,\perp} , \tag{4}$$

$$x = (\varepsilon_{\mathrm{d}} - \varepsilon_{\mathrm{h}})[\varepsilon_{\mathrm{m}} L_1 + \varepsilon_{\mathrm{d}}(1 - L_1)] + Q(\varepsilon_{\mathrm{m}} - \varepsilon_{\mathrm{d}})[\varepsilon_{\mathrm{d}}(1 - L_2) + \varepsilon_{\mathrm{h}} L_2] ,$$

$$y = [\varepsilon_{\mathrm{d}} L_2 + \varepsilon_{\mathrm{h}}(1 - L_2)][\varepsilon_{\mathrm{m}} L_1 + \varepsilon_{\mathrm{d}}(1 - L_1)] + Q(\varepsilon_{\mathrm{m}} - \varepsilon_{\mathrm{d}})(\varepsilon_{\mathrm{d}} - \varepsilon_{\mathrm{h}}) L_2(1 - L_2),$$

where Q is the ratio of the volume of the core to the volume of the coated particle ($= V_1/V_2$), through which the size of the particle and the thickness of the adsorbed layer can be incorporated into the calculation. The depolarization factors of the core and the coated ellipsoid (L_1 and L_2, respectively) are solely a function of the aspect ratio of the ellipsoid η ($= a/b$; a and b are the radius along the major and minor axes of the ellipsoid, respectively) [67]. The subscripts $\parallel$ and $\perp$ refer to the cases where the applied electric field of the incident light is parallel ($\parallel$) and perpendicular ($\perp$), respectively, to the substrate surface.

The MG model includes weak interactions between the islands only through the Lorentz field and thus provides a good description for very thin island films in which the metal islands are well separated from each other. When the islands are densely packed (i.e. for thicker island films), dipole interactions between islands cannot be neglected. In such a case, the BR model provides a better approximation. In the BR model, the effective dielectric function is represented as [63]

$$\varepsilon_{\mathrm{BR}} = \varepsilon_{\mathrm{h}} \frac{3(1 - F) + F\alpha'}{3(1 - F) - 2F\alpha'} , \tag{5}$$

This model assumes that the metal islands are embedded in the effective medium [65]. Thus, α and ε_{h} in (5) must be replaced by α' and $\varepsilon_{\mathrm{BR}}$, respectively, in this case.

Transmission spectra of a model molecule layer on 5 and 8 nm thick Ag island films simulated with both the MG and the BR models, are shown by the solid curves in Fig. 4 [26]. The thickness of the adsorbed molecular layer and the particle size ($2a$) were assumed to be 1 and 25 nm, respectively. The filling factors were taken from experimental data [68]. The dielectric function of Ag was calculated from the Drude model,

$$\varepsilon_{\mathrm{m}}(\omega) = 1 - \frac{\omega_{\mathrm{p}}^2}{\omega(\omega + \mathrm{i}/\tau)}\,, \tag{6}$$

where the plasma frequency ω_{p} equals 1.15×10^{16} s^{-1} and the relaxation time τ is 1×10^{-15} s for Ag [69]. The dielectric function of the adsorbed molecule was approximated by a damped harmonic dipole given by

$$\begin{aligned}
\varepsilon_{\mathrm{d}}(\nu) &= \varepsilon'(\nu) + \varepsilon''(\nu)\,,\\
\varepsilon'(\nu) &= n_\infty^2 + \frac{B(\nu_0^2 - \nu^2)}{(\nu_0^2 - \nu^2)^2 + \gamma^2\nu^2}\,,\\
\varepsilon''(\nu) &= \frac{B\gamma\nu}{(\nu_0^2 - \nu^2)^2 + \gamma^2\nu^2}\,,
\end{aligned} \tag{7}$$

where ν is the frequency in wavenumbers (cm^{-1}), n_∞ is the refractive index at a frequency far from the band center ν_0, and γ is the bandwidth. B is a constant related to the band intensity. These parameters were tentatively

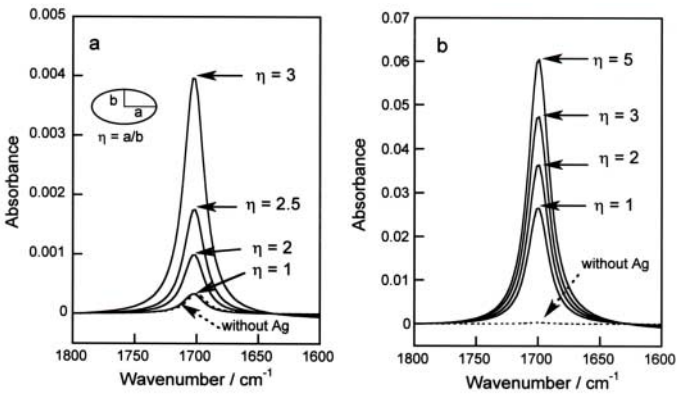

Fig. 4. SEIRA spectra of a model molecule adsorbed on Ag island films simulated by using the Maxwell-Garnett (**a**) and Bruggemann (**b**) effective-medium models. The mass thickness of the Ag film is 5 nm for (**a**) and 8 nm for (**b**). The *dashed trace* is the spectrum of a molecular layer on the substrate (CaF_2) without a metal film. η represents the aspect ratio of the metal ellipsoid (Fig. 2). See text for details

assumed to be $n_\infty = 1.77$, $B = 30000\,\mathrm{cm}^{-2}$, $\nu_0 = 1700\,\mathrm{cm}^{-1}$, and $\gamma = 20\,\mathrm{cm}^{-1}$.

The dashed spectra in the figure correspond to a molecular layer formed directly on the substrate (CaF_2) without a metal film. The simulations clearly demonstrate that the molecular vibrations are observable very strongly in the presence of metal islands and that the enhancement depends on the shape of the islands (i.e. on η). For the 5 nm thick Ag film (Fig. 4a), the intensity for $\eta = 1$ (sphere) is as small as that without metal islands, but increases with η. For $\eta = 3$ (a typical value for vacuum-evaporated 5 nm thick Ag films), the enhancement factor, defined by the ratio of band intensities with and without a metal, is about 15. Larger enhancement factors are calculated with the BR model for the 8 nm thick Ag film (Fig. 4b). This factor reaches about 150 for $\eta = 3$. Such a large enhancement cannot be calculated if the MG model is used instead of the BR model, implying that interactions between metal islands play an important role in SEIRA. This result may be consistent with the fact that the tail of the collective electron resonance extends well into the mid-infrared region for thicker films owing to the dipole interactions between the islands (Fig. 3).

The enhancement factors calculated here are slightly smaller than the experimental values for the symmetric NO_2 stretching mode of p-nitrobenzoate adsorbed on Ag island films (about 50 and 500 at Ag thickness of 5 and 8 nm, respectively) [10]. Since this molecule is known to be oriented with the C_2 axis perpendicular to the surface, an enhancement factor of (15–150) × 3 = 45–450 can be calculated for this mode by taking the orientation effect into account. This value is in reasonable agreement with the experiments.

The EM model can also simulate well some SEIRA spectra measured with the ATR and external-reflection geometries [11,70].

Despite the large simplification, the EM model explains well several characters intrinsic to SEIRA. The solid curve in Fig. 5 shows the band intensity of a model molecular layer calculated with the MG EMA as a functionof its thickness (d_{mol}) [35]. The intensity rises sharply as d_{mol} increases and then decreases slightly, whereas it increases linearly with d_{mol} on a metal-free substrate, as shown by the dashed line (the Lambert–Beer law). The result clearly demonstrates that the enhancement is a short-range effect limited to a few nanometers away from the surface. It should be noted that the EM simulation can be applied only to small d_{mol} values, because the voids between metal islands are completely filled with molecules at a certain d_{mol} and further deposited molecules form an overlayer on the composite layer. Hence, the experimentally observable curve of intensity versus d_{mol} should be the sum of the solid curve and the dashed line. The simulation is in good agreement with several experiments [10,22,23,24,25].

SERS, which is observed in the visible and near-infrared regions, is significant on free-electron metals (Au, Ag, and Cu) but is hardly observable on transition metals owing to the strong damping of plasmon modes (i.e. the

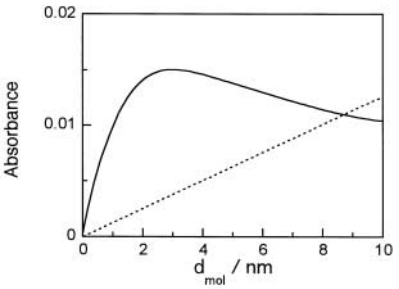

Fig. 5. Simulated peak intensity of a model molecule on a 5 nm thick Au island film plotted as a function of the thickness of the molecular layer, d_{mol}. The *dashed line* is the result without the metal film. The experimentally observable dependence of the band intensity on d_{mol} represented by the sum of the two components shown

large imaginary part of the dielectric constant) [1,2,3]. In contrast, the EM calculations predict an enhancement of infrared absorption on transition metals as strong as that on coinage metals [26]. In fact, several recent experiments have demonstrated the SEIRA effect on many other metals such as Pt, Pd, Rh, Ru, Ir, Sn, Fe, In, Pb, and Pt–Fe alloys [16,17,19,32,49,50,70,71,72,73]. Since the dielectric constants of these metals do not differ greatly from those of coinage metals in the infrared region, these results may be a reasonable consequence.

Asymmetric and bipolar (i.e. derivative-like) band shapes are often observed in SEIRA spectra [19,32,49]. In some cases, molecular vibrations are observed as negative absorption peaks, i.e. as reflectance maxima [16,17,19]. Very recently, it has been demonstrated that such spectral features can be simulated with the an EM calculation using the Bergman EMA [19].

2.2 Chemical Mechanisms

Molecules chemisorbed on a metal surface show a larger enhancement than do physisorbed molecules, suggesting some chemical effect between the molecule and the surface. It is known that the absorption coefficients of chemisorbed molecules are larger than those of condensed overlayers [38]. Interactions between adsorbed molecules also affect the intensity [36,37]. Some theories predict that charge oscillations between molecular orbitals and the metal surface enlarge the absorption coefficients of adsorbates by 'intensity borrowing' from the charge-oscillations [36,37,74]. There exist some experimental results that seem to support such chemical mechanism [32,75,76]. For example, CO adsorbed on Fe island films evaporated on MgO(001) shows a very asymmetric SEIRA band [32]. An enhancement factor of about 100 was estimated for this system. The band shape and enhancement were theoretically explained by assuming a Fano-type resonance of the molecular vibration with electronic transitions between the metal and the adsorbate [32]. The simulation agrees

quite well with the observed spectra and the enhancement factor of 100 was ascribed to the chemical origin. Nevertheless, it should be noted that the asymmetric band shape can be explained also by an EM mechanism [19] as described previously. In addition, the chemical enhancement factor of 100 is one order of magnitude larger than that observed for CO on bulk metal surfaces (where the factor is less than 10). Although the difference in the electronic conditions between the island metal surface and the bulk metal surface might have a strong effect on the enhancement, the details are still unclear. Further theoretical and experimental studies of the chemical mechanism are necessary.

3 Electrochemical Dynamics Monitored by SEIRAS

Recent research in electrochemistry has increasingly involved the use of surface-sensitive analytical techniques in combination with conventional electrochemical techniques. The chief reason for this development is that electrochemical techniques inevitably measure the sum of all surface processes. The results primarily provide kinetic information, and no direct molecular information on the species involved in the reactions can be obtained. SEIRAS has been applied very successfully to examine molecular events occurring at the electrochemical interface. The achievements before 1997 have been reviewed in [8]. In this section, the basic aspects of this technique are summarized first and then some recent developments are described.

3.1 Experimental Technique

So far, the so-called infrared reflection absorption spectroscopy (IR-RAS) technique (Fig. 6a) has been used for in situ infrared studies of the electrochemical interface [77]. P-polarized infrared radiation passing through the solution phase is reflected at the electrode surface at a high incidence angle. The working electrode is pushed against an infrared-transparent cell window to reduce the strong absorption of the electrolyte solution. The thickness of the solution layer between the electrode and the window is typically 1–10 μm. An advantage of this technique is that well-defined single-crystals can be used as working electrodes, as well as poly-crystals. However, this technique has two serious problems when it is used for dynamic studies. One is that the thin-layer structure of the cell prevents mass transportation between the thin-layer and the reservoir, and the system does not respond quickly to changes of the externally applied potential owing to the large solution resistance. Hence, this technique can be used only under static or quasi-static conditions. The other is the interference from the bulk solution. Although the solution layer is very thin, it is still much thicker than a monolayer on the electrode. Thus the signal from the adsorbate is superposed on the solution background, which is about three orders of magnitude stronger. The

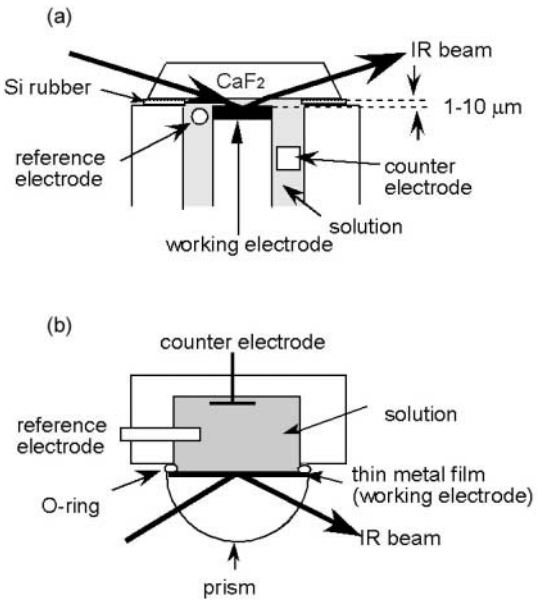

Fig. 6. In situ monitoring of the electrochemical interface with IR-RAS (**a**) and ATR-SEIRAS (**b**)

solution background can be removed to a large extent by measuring potential difference spectra [77], but its complete subtraction is very difficult.

These problems intrinsic to IR-RAS can be removed by using the ATR configuration illustrated in Fig. 6b. A thin metal film deposited on a prism (Si, Ge, or ZnSe) is used as the working electrode. The infrared radiation passed through the prism is totally reflected at the electrode/electrolyte interface. Since the evanescent wave penetrates only a few hundred nanometers into the solution phase [78], it is not necessary for the solution phase to be thin and further the solution background can be significantly reduced compared with that in IR-RAS. On the contrary, the absorption of species adsorbed on the electrode surface is enhanced by the SEIRA effect. Consequently, the signals from the adsorbate and solution are comparable in this configuration, which facilitates the complete subtraction of the solution background [70].

The details of the experimental setup and procedures have been described in [70,79]. Although the electrodes used in ATR-SEIRAS must be island films, relatively thick (15–20 nm) island films prepared by vacuum evaporation have a conductivity good enough for electrochemistry. It should be noted that slow deposition of the metal is crucial in preparing SEIRA-active thin-film electrodes by vacuum evaporation [15]. Evaporated metal films are generally polycrystalline, except for Au. The Au surface has a tendency such that facets with (111) crystallographic orientation preferentially appear on the surface when it is evaporated very slowly. A short (about 10 s) annealing of the film

with a hydrogen–oxygen flame accelerates the recrystallization of the surface toward the (111) orientation [80]. A prolonged annealing of the film generally reduces the enhancement. The electrodes are used after cleaning their surface in the solution by repeated potential sweeps between the surface oxidation and hydrogen evolution potentials. Oxidation–reduction cycles in solutions containing halogen ions, which are very often used for observing SERS [1,3], are not recommended, to avoid complex electrochemistry. The surface can be kept clean for several hours if ultrapure water and chemicals are used.

3.2 Comparison of ATR-SEIRAS and IR-RAS

The ATR-SEIRAS technique has been applied very successfully to several electrochemical systems [8,28,29,30,49,50,56,57,58,80,81,82,83]. To highlight the difference between IR-RAS and ATR-SEIRAS, infrared spectra of pyridine adsorbed on Au electrodes measured with the two techniques [28,84] are compared in Fig. 8. The electrode used in the IR-RAS measurements was an Au(111) single-crystal, whereas in the ATR-SEIRAS measurement it was a vacuum-evaporated preferentially (111)-oriented 20 nm thick Au film. The infrared reflection absorption (IR-RA) spectra are represented by the relative reflectance change, defined as $\Delta R/R = (R_{\mathrm{sample}} - R_{\mathrm{ref}})/R_{\mathrm{ref}}$, where R_{sample} and R_{ref} are the reflectivities of the electrode at the sample and reference potentials, respectively. On the other hand, the ATR spectra are represented in absorbance units, defined by $A = -\log(R_{\mathrm{sample}}/R_{\mathrm{ref}})$. In both measurements, the reference potential was –0.75 V versus a saturated calomel electrode (SCE), at which potential the molecule is totally desorbed from the surface. Therefore, the adsorbate on the electrodes gives down-going bands in the IR-RA spectra and up-going bands in the SEIRA spectra.

Several adsorbate bands are clearly identifiable in both sets of spectra, but the band intensities in the ATR spectra are about 20 times greater than those in the IR-RA spectra. Note that $\Delta R/R = 0.0005$ corresponds to 0.0002 absorbance units. Of course, the difference in surface area between the single-crystal and island film electrodes contributes to the different intensities. However, the roughness factor of the island film, estimated by electrochemical techniques, was only about 2.5. Considering that IR-RAS has a sensitivity over 10 times higher than transmission spectroscopy [27], an enhancement factor of about 100 or more is estimated for the evaporated Au electrode.

The IR-RA spectrum is characterized by a strong up-going band at 1445 cm^{-1}. Since the adsorption of the molecule onto the electrode surface reduces its concentration in the thin solution layer, the up-going band is ascribed to pyridine in the solution. Pyridine in the solution has another strong band at 1594 cm^{-1}, which deforms the spectral features around 1600 cm^{-1}. The down-going band at 1601 cm^{-1} is a ghost produced by the superposition of the up-going solution band at 1594 cm^{-1} and down-going band of adsorbed pyridine at 1593 cm^{-1}.

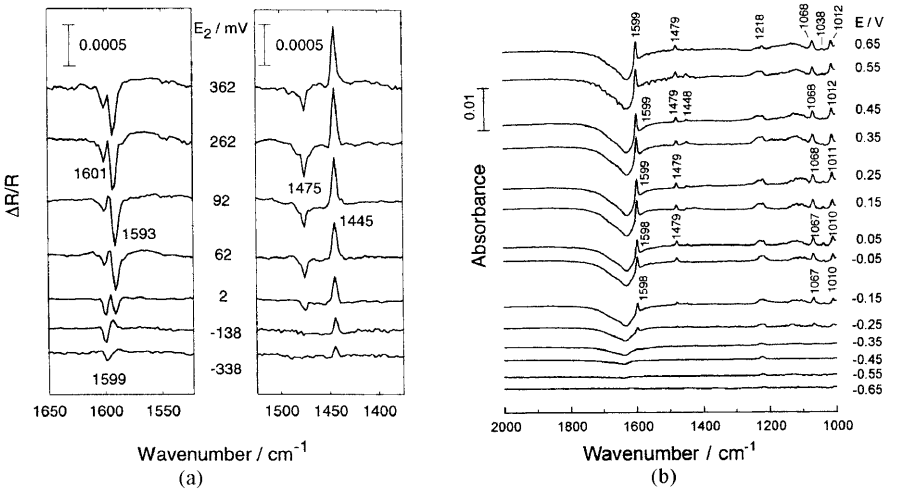

Fig. 7. IR-RA and ATR-SEIRA spectra of pyridine adsorbed on an Au(111) single-crystal electrode (**a**) [84] and on a vacuum-evaporated (111)-oriented 20 nm thick Au film electrode (**b**) [29], respectively. Solutions: (**a**) 0.1 M $KClO_4$ + 3 mM pyridine, (**b**) 0.1 M $NaClO_4$ + 1 mM pyridine. The Reference potential was 0.75 V versus SCE in both measurements

The ATR-SEIRAS technique is free from this problem and only the vibrational modes of adsorbed pyridine are observed owing to its higher surface-sensitivity. Even the very weak band at 1448 cm^{-1} located very close to the solution band can be identified. In the SEIRA spectrum, a very broad negative-going band, assignable to the bending mode of water, is observed at 1620 cm^{-1}, which is not seen in the IR-RA spectrum because D_2O was used as the solvent to avoid strong interference from the solution. This band decreases in intensity with increasing potential, concomitantly with the growth of the pyridine bands. Thus, this band can be ascribed to water molecules that were removed from the interface by pyridine adsorption. This explanation is supported by the considerably lower frequency of this band than that of bulk water (1645 cm^{-1}) [79,81]. The observation of water molecules at the interface also demonstrates the high surface-sensitivity of this technique.

In summary, the ATR-SEIRAS technique is useful for observing only the interface without interference from the solution. On the other hand, IR-RAS can provides information on molecules both at the interface and in the bulk solution, although the superposition of the bands of both species often makes the spectral analysis difficult except in cases where the spectrum of the adsorbate is greatly changed by adsorption.

When solution bands are well separated from adsorbate bands, they can be used for semi-quantitative estimation of the amount of molecules adsorbed on the surface [84]. The intensity of the 1445 cm^{-1} band in Fig. 7a was shown

to be proportional to the Gibbs surface excess (Γ) of pyridine determined by chronocoulometry.

On the other hand, the intensities of adsorbate bands are usually not proportional to the surface coverage, as shown in Fig. 8. The intensity of the 1597 cm^{-1} band in Fig. 7b (circles in Fig. 8) does not track the Γ versus potential curve (solid line) [85]. Although pyridine adsorption occurs at potentials more positive than –0.7 V, this band is observed at potentials more positive than –0.4 V, where Γ reaches a plateau. On the basis of the surface selection rule, the result is interpreted as showing that the pyridine ring is parallel to the surface at negative potentials and rises up as the potential increases. This potential-dependent reorientation of pyridine deduced by SEIRAS has been confirmed by in situ scanning tunneling microscopy [28].

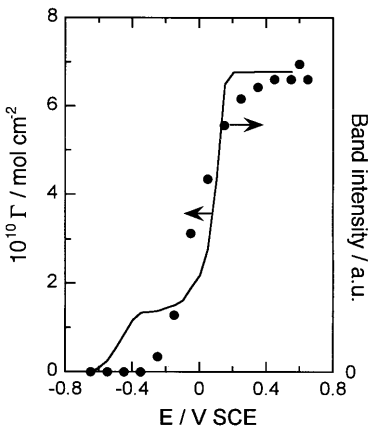

Fig. 8. The intensity of the 1599 cm^{-1} band in Fig. 7b plotted as a function of the potential (*circles*). The solid line represents the Gibbs surface excess (Γ) of pyridine measured as a function of the applied potential, which was taken from [85]

3.3 Time-Resolved Monitoring of Electrode Dynamics

Since the signal-to-noise ratio of a spectrum is proportional to the square root of the number of interferograms added together (in the case of FT-IR spectroscopy), one will recognize immediately that the high sensitivity of ATR-SEIRAS facilitates real-time or time-resolved monitoring of dynamic processes at the interface. The quick response of the electrochemical cell in the ATR configuration is also quite convenient for such measurements. In general, a signal-to-noise ratio good enough for detailed analysis of monolayer adsorbates can be obtained by adding fewer than 50 interferograms, which requires acquisition times of less than 10 s for most FT-IR spectrometers. For strongly absorbing molecules, high-quality spectra can be obtained

without addition of interferograms. The short acquisition time enables us to accumulate a series of spectra successively under potential-sweep conditions together with electrochemical data. If the reactions to be investigated are reversible or repeatable, they can be monitored with microsecond time-resolution by using a step–scan FT-IR technique [54,56,58]. By applying two-dimensional correlation analysis (i.e. the so-called 2D-IR analysis) to a series of time-resolved spectra, detailed information on the reactions and dynamics that is not readily accessible with conventional one-dimensional spectra can be extracted [55,81].

A comparison of spectral and electrochemical data is quite important for obtaining deeper insights into electrochemistry [25,28,29,56,58,82]. As an example, a time-resolved SEIRA study of underpotential deposition of Cu on an Au(111) surface is shown in Fig. 9 [58]. Underpotential deposition is a phenomenon in which a monolayer or submonolayer amount of metal atoms is adsorbed on the surfaces of a different metal at a potential more positive than the equilibrium potentials. The inset in Fig. 9a shows a typical cyclic voltammogram for an Au(111) electrode in 0.1 M H_2SO_4 containing 1 mM

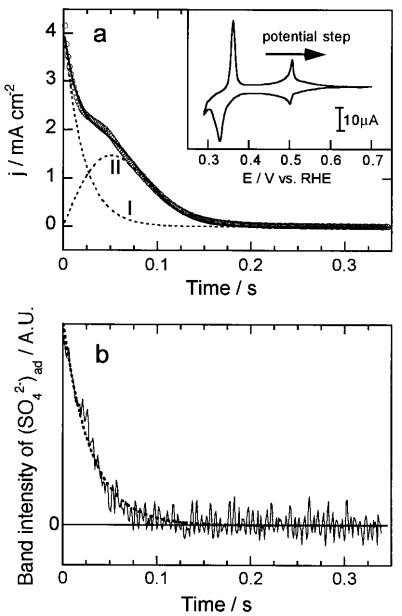

Fig. 9. (**a**) Current transient for a potential step from 0.45 to 0.6 V at an Au(111) electrode in 0.1 M H_2SO_4 containing 1 mM $CuSO_4$, and (**b**) the simultaneously measured transient of the band intensity of sulfate adsorbed on the electrode. The infrared data were taken from a series of ATR-SEIRA spectra measured with a 1 ms time-resolution. The *inset* shows a cyclic voltammogram recorded at a scan rate of $2\,\mathrm{mVs}^{-1}$

$CuSO_4$. Adsorption and desorption of Cu adatoms and sulfate ions provides the current flow. The sharp cathodic peaks at 0.5 and 0.33 V correspond to the formation of well-ordered phases. The two anodic peaks correspond to the reverse processes. The ordered phase formed in the potential range between 0.4 and 0.5 V is called the honeycomb ($\sqrt{3} \times \sqrt{3}$) phase, in which two-thirds of a monolayer (ML) amount of Cu adatoms are arranged in a honeycomb structure and one-third of a monolayer ML amount of sulfate anions are coadsorbed in the center of the honeycomb (see Fig. 10).

Figure 9a shows the current transient for the dissolution of the honeycomb ($\sqrt{3}\times\sqrt{3}$) phase triggered by a potential step from 0.45 to 0.6 V. The transient curve can be simulated by a combination of two kinetic terms as follows:

$$j(t) = k_1 \exp(-k_2 t) + k_3 t \exp(-k_4 t^2)\,. \tag{8}$$

The first term (curve I) corresponds to a Langmuir (i.e. random) process, and the second term (curve II) to a nucleation-and-growth process. The time constants k_2 and k_4 are 49 s^{-1} and 193 s^{-2}, respectively. This simulation indicates that the dissolution of the honeycomb ($\sqrt{3}\times\sqrt{3}$) phase takes place via two different successive processes, but conventional electrochemical measurements do not provide any detailed molecular information on these processes. Figure 9b represents the corresponding transient of the band intensity of coadsorbing sulfate, which was taken from a series of SEIRA spectra measured with a time-resolution of 1 ms. This transient can be simulated with a

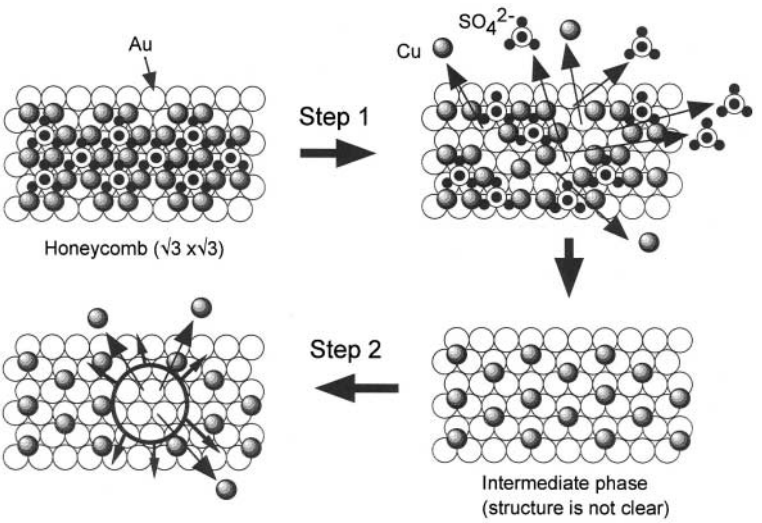

Fig. 10. Schematic representation of the dissolution dynamics of the honeycomb ($\sqrt{3} \times \sqrt{3}$) phase on an Au(111) electrode surface deduced from the data shown in Fig. 9. One half of the Cu adatoms and all sulfate ions are desorbed in step 1 with Langmuir kinetics. The remaining half of the Cu adatoms are desorbed in step 2 with nucleation-and-growth kinetics

single Langmuir term with a rate constant of 35 s^{-1}, which is nearly identical to that of the first process found in the current transient. The results indicate that sulfate ions are totally desorbed from the surface in the initial process and that the subsequent process involves desorption of Cu adatoms only. By integrating curves I and II in Fig. 9a, the charge densities passing during the first and second processes have been measured to be 85 and 125 μC cm^{-2}, respectively. A charge density of 125 μC cm^{-2} corresponds to that required for desorption of 1/3 ML of Cu adatoms (one-half of the Cu adatoms in the honeycomb phase). Accordingly, it is concluded that 1/3 ML of Cu and all sulfate ions are desorbed in the initial process, and then the remaining 1/3 ML of Cu adatoms is desorbed in the subsequent process. The smaller charge density of 85 μC cm^{-2} for the initial process is accounted by the superposition of a negative charge of 40 μC cm^{-2} required for desorption of the sulfate. The processes are schematically represented in Fig. 10.

3.4 A New Approach to Electrode Dynamics

When the electrode potential is changed, current flows across the interface to charge-up the double-layer. The time-constant for the double-layer charging is typically a few milliseconds for electrodes of ordinary size (millimeter to centimeter in diameter). Owing to the interference from the double-layer charging current, reactions that have time-constants equivalent to or smaller than that of the double-layer charging cannot be examined by conventional electrochemical techniques. Fortunately, spectroscopic measurements are not interfered with by the double-layer charging. Molecular absorption/desorption at electrodes within the time-region of the double-layer charging has been investigated by ATR-SEIRAS with a 100 μs time-resolution [56]. The change of the actual potential across the interface during the double-layer charging has also been measured from spectral changes of a SAM of 4-mercaptopyridine on Au [57].

Since electrochemical reactions are limited by double-layer charging, diffusion, and several other slow processes, it is impossible to determine rate constants of faster processes by any time-domain approaches. To overcome this limitation, measurements in the frequency domain are often used in electrochemistry. In ac impedance spectroscopy, for example, the potential is modulated and the phase shift of the corresponding current flow with respect to the modulation is measured, from which kinetic parameters can be obtained. However, reactions with rate constants larger than $\sim 10^3 s^{-1}$ cannot be measured even with this method, owing to the double-layer charging. Since spectroscopic measurements are not interfered with by the double-layer charging, very fast processes should be accessible if electrochemical measurements are replaced by spectroscopic measurements. This idea has been realized in the UV–visible region [86]. Unfortunately, the molecular specificity of UV–visible spectroscopy is not high enough. The use of FT-IR spectroscopy has

also been examined for this purpose [87,88]. However, the relatively low sensitivity of infrared spectroscopy, the thin-layer structure of the electrochemical cell, and some other technical problems have prevented its practical use. Very recently, these problems were removed by coupling potential-modulated FT-IR with ATR-SEIRAS [57].

A block diagram of the experimental setup used for potential-modulated FT-IR spectroscopy is shown in Fig. 11. The electrode potential is modulated with a sinusoidal wave generated by a waveform generator, and the in-phase and quadrature (90° out-of-phase) components of the modulated IR signal are analyzed with a lock-in-amplifier. The dc component of the signal is used as the reference. The crosstalk between Fourier frequencies and the potential modulation frequency can be removed by the use of a step–scan FT-IR spectrometer.

Typical potential-modulated spectra for a 4-mercaptopyridine SAM on an Au electrode are shown in Fig. 12. The solid and dashed curves correspond to the in-phase and quadrature spectra, respectively. The bipolar band around 1470 cm^{-1} implies a shift of the vibrational frequency with potential. On the other hand, the 1618 cm^{-1} band changes only in its intensity. The peak intensities of the 1618 cm^{-1} band in the in-phase and quadrature spectra measured at modulation frequencies ranging from 41 Hz to 50 kHz form a semicircle in the complex plot (Cole–Cole plot), as in the Cole–Cole plots of ac impedance. A theoretical analysis of the infrared data revealed that the spectral changes occur at a rate of $\sim 5 \times 10^5 s^{-1}$, which is much larger than the time constant of the double-layer charging ($1.9 \times 10^3 s^{-1}$) [57].

Potential-dependent spectral changes, as shown in Fig. 12, are observed for many molecules adsorbed on electrode surfaces. Two mechanisms have been proposed for CO, the Stark-tuning and back-donation models [77]. The Stark-tuning model predicts that the change of the electric field across the double-layer changes the vibrational properties of the adsorbate. The back-donation model predicts that the change in the potential (that is, the Fermi

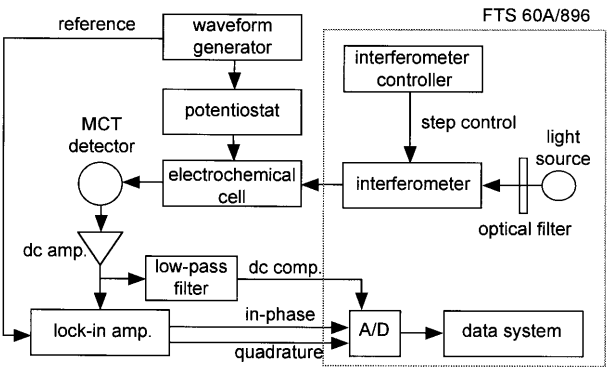

Fig. 11. Experimental setup for potential-modulated FT-IR spectroscopy

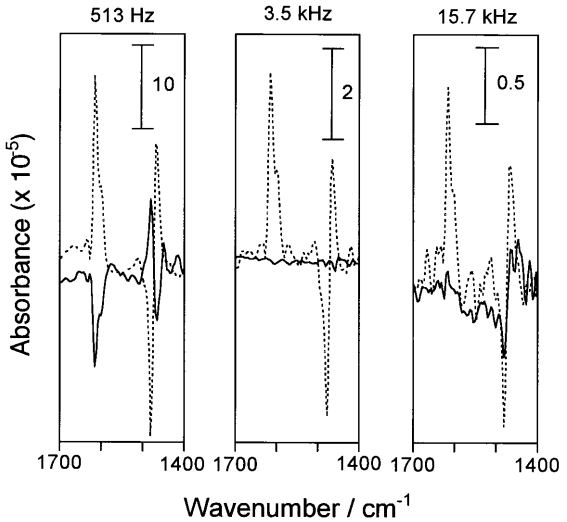

Fig. 12. In-phase (*solid lines*) and quadrature (*dashed lines*) spectra of a 4-mercaptopyridine self-assembled monolayer on an Au thin-film electrode in 0.1 M $HClO_4$ measured by potential-modulated FT-IR spectroscopy at the modulation frequencies indicated in the figure

level of the electrode surface) changes the amount of charge back-donated from the metal to the $2\pi^*$ orbital of CO, resulting in the spectral changes. If the Stark-tuning effect is dominant, the rate of the spectral changes should be the same as that of the double-layer charging (i.e. of the actual potential change at the interface). If this is not the case, the rate may be different (presumably, much faster). In the case of 4-mercaptopyridine, the rate of the spectral changes is much faster than that of the double-layer charging, indicating that the charge-transfer mechanism rather than the Stark-tuning mechanism contributes to the spectral changes.

4 Summary and Remarks

In summary, SEIRA is a phenomenon similar to SERS and is characterized by a 10–1000 times enhancement of the infrared absorption of molecules adsorbed on metal island films or small metal particles. The local electric field around the metal islands produced by the coupling of the incident photon field with the metal excites an adsorbed molecule. The excited molecule perturbs the optical properties of the metal, and the molecular vibrations are observed through a change of the transmittance or reflectance of the island film. Since the absorption coefficient and volume fraction of the metal are larger than those of the molecules, the molecular vibrations can be observed more strongly than would be expected from conventional measurements with-

out the metal. Molecular vibrations that change the dipole moment along the surface normal are selectively enhanced. Preferential orientation of the molecules on the surface provides an additional enhancement by a factor of three at maximum. Chemical interactions of molecules with the surface can give additional enhancement, but the details are still unclear. Among several applications, SEIRAS has been applied most successfully to electrochemical systems. Thanks to developments in FT-IR instrumentation and data analysis techniques such as 2D-IR, SEIRAS has enabled us to study electrode dynamics that is not readily accessible by conventional electrochemical techniques.

Despite twenty years of history, SEIRA has received less attention than SERS. This is probably due to the smaller enhancement factor of SEIRA. However, infrared spectroscopy basically has a higher sensitivity than Raman spectroscopy, and hence the sensitivities of SEIRAS and SERS are comparable. It is emphasized that SEIRAS and SERS are not competitive but are supplementary to one other, as in the case of normal infrared and Raman spectroscopy. A comparison of SEIRA and SERS spectra is very helpful for detailed analysis of both spectra [42,44,72]. The use of SEIRAS in tandem with other analytical techniques will also be very fruitful for surface chemistry and surface electrochemistry, as described in Sect. 3.2. In electrochemistry, the combined use of SEIRAS and STM is becoming popular [28,29,30,83,89].

References

1. R. K. Chang , T. E. Furtak, *Surface Enhanced Raman Scattering* (Plenum, New York 1982) 163, 164, 167, 171, 174
2. H. Metiu, Surface Enhanced Spectroscopy, Prog. Surf. Sci. **17**, 153-320 (1984) 163, 164, 165, 167, 171
3. M. Moskovits, Surface-enhanced spectroscopy, Rev. Mod. Phys. **57**, 783–826 (1985) 163, 164, 165, 167, 171, 174
4. A. Otto, I. Mrozeck, H. Grabhorn, W. Akemann, Surface-enhanced Raman scattering, J. Phys. Condens. Matter **4**, 1143–1212 (1992) 163, 164, 167
5. A. Hartstein, J. R. Kirtley, J. C. Tsang, Enhancement in the infrared absorption from molecular monolayers with thin metal overlayers, Phys. Rev. Lett. **45**, 201–204 (1980) 163
6. A. Hatta, T. Ohshima, W. Suëtaka, Observation of the enhanced infrared absorption of p-nitrobenzoate on Ag island films with an ATR technique, J. Appl. Phys. A **29**, 71–75 (1982) 163
7. A. Hatta, Y. Suzuki, W. Suëtaka, Infrared absorption enhancement of monolayer species on thin evaporated Ag films by use of a Kretschmann configuration, Evidence for two types of enhanced surface electric fields, Appl. Phys. A **35**, 135–140 (1984) 163
8. M. Osawa, Dynamic processes in electrochemical reactions studied by surface-enhanced infrared absorption spectroscopy (SEIRAS), Bull. Chem. Soc. Jpn. **70**, 2861–2880 (1997) 163, 164, 165, 172, 174

9. Y. Nishikawa, K. Fujiwara, T. Shima, A Study of the qualitative and quantitative analysis of nanogram samples by transmission infrared spectroscopy with the use of silver island films, Appl. Spectrosc. **45**, 747–751 (1991) 163, 164
10. M. Osawa, M. Ikeda, Surface-enhanced infrared absorption of p-nitrobenzoic acid deposited on silver island films: contribution of electromagnetic and chemical mechanisms, J. Phys. Chem. **95**, 9914–9919 (1991) 163, 164, 166, 167, 170
11. Y. Nishikawa, K. Fujiwara, K. Ataka, M. Osawa, Surface-enhanced external reflection spectroscopy at low reflective surfaces and its application to surface analysis of semiconductors, glasses, and polymers, Anal. Chem. **65**, 556–562 (1993) 163, 165, 170
12. S. J. Lee, K. Kim, Diffuse reflectance infrared spectra of stearic acid self–assembled on fine silver particles, Vib. Spectrosc. **18**, 187–201 (1998) 163
13. M. Osawa, M. Kuramitsu, A. Hatta, W. Suëtaka, H. Seki, Electromagnetic effect in enhanced infrared absorption of adsorbed molecules on thin metal films, Surf. Sci. Lett. **175**, L787–L793 (1986) 163, 167
14. Y. Suzuki, M. Osawa, A. Hatta, W. Suëtaka, Mechanism of absorption enhancement in infrared ATR spectra observed in the Kretschmann configuration, Appl. Surf. Sci. **33/34**, 875–881 (1988) 163, 167
15. Y. Nishikawa, T. Nagasawa, K. Fujiwara, M. Osawa, Silver island films for surface-enhanced infrared absorption spectroscopy: effect of island morphology on the absorption enhancement, Vib. Spectrosc. **6**, 43–53 (1993) 163, 164, 165, 173
16. G.-Q. Lu, S.-G. Sun, S. P. Chen, L.-R. Cai, Novel properties of dispersed Pt and Pd thin layers supported on GC for CO adsorption studied using in situ MS–FTIR reflection spectroscopy, J. Electroanal. Chem. **421**, 19–23 (1997) 163, 165, 171
17. G.-Q. Lu, S.-G. Sun, L.-R. Cai, S.-P. Chen, Z.-W. Tian, In situ FTIR spectroscopic studies of adsorption of CO, SCN–, and poly(o–phenylenediamine) on electrodes of nanometer thin films of Pt, Pd, and Rh: Abnormal infrared effects (AIREs), Langmuir **16**, 778–786 (2000) 163, 165, 171
18. H. D. Wanzenböck, B. Mizaikoff, N. Weissenbacher, R. Kellner, Surface enhanced infrared absorption spectroscopy (SEIRA) using external reflection on low-cost substrates, Fresenius J. Anal. Chem. **362**, 15–20 (1998) 163, 165
19. A. E. Bjerke, P. R. Griffiths, W. Theiss, Surface-enhanced infrared absorption of CO on platinized platinum, Anal. Chem. **71**, 1967–1974 (1999) 163, 165, 171, 172
20. S. Y. Kang, I. C. Jeon, K. Kim, Infrared absorption enhancement at silver colloidal particles, Appl. Spectrosc. **52**, 278–283 (1998) 163
21. J. A. Seelenbinder, C. W. Brown, P. Pivarnik, A. G. Rand, Colloidal gold filtrates as a metal substrates for surface-enhanced infrared absorption spectroscopy, Anal. Chem. **71**, 1963–1966 (1999) 163
22. T. Kamata, A. Kato, J. Umemura, T. Takenaka, Intensity enhancement of infrared attenuated total reflection spectra of stearic acid Langmuir–Blodgett monolayers with evaporated silver island films, Langmuir **3**, 1150–1154 (1987) 164, 165, 170
23. A. Hatta, N. Suzuki, Y. Suzuki, W. Suëtaka, Infrared absorption of polycyanoacrylate enhanced by Ag island films in the Kretschmann's ATR geometry, The coverage dependence, Appl. Surf. Sci. **37**, 299–305 (1989) 164, 170

24. E. Johnson, R. Aroca, Surface-enhanced infrared spectroscopy of monolayers, J. Phys. Chem. **99**, 9325–9330 (1995) 164, 170
25. M. Osawa, K. Yoshii, In situ and real–time surface-enhanced infrared study of electrochemical reactions, Appl. Spectrosc. **51**, 512–518 (1997) 164, 165, 170, 177
26. M. Osawa, K. Ataka, K. Yoshii, Y. Nishikawa, Surface-enhanced infrared spectroscopy: the origin of the absorption enhancement and band selection rule in the infrared spectra of molecules adsorbed on fine metal particles, Appl. Spectrosc. **47**, 1497–1502 (1993) 164, 169, 171
27. F. M. Hoffmann, Infrared reflection-absorption spectroscopy of adsorbed molecules, Surf. Sci. Rep. **3**, 107-192 (1983) 164, 174
28. W.-B. Cai, L.-J. Wan, H. Noda, Y. Hibino, K. Ataka, M. Osawa, Orientational phase transition in a pyridine adlayer on gold(111), Langmuir **14**, 6992–6998 (1998) 164, 174, 176, 177, 182
29. H. Noda, T. Minoha, L.-J. Wan, M. Osawa, Adsorption and ordered phase formation of 2,2'-bypyridine on Au(111): a combined surface-enhanced infrared and STM study, J. Electroanal. Chem. **481**, 62–68 (2000) 164, 174, 175, 177, 182
30. L.-J. Wan, M. Terashima, H. Noda, M. Osawa, Molecular orientation and ordered structure of benzenethiol adsorbed on gold(111), J. Phys. Chem. B **104**, 3563–3569 (2000) 164, 174, 182
31. G. T. Merklin, P. R. Griffith, Influence of chemical interactions on the surface-enhanced infrared absorption spectrometry of nitrophenols on copper and silver films, Langmuir **13**, 6159–6163 (1997) 164
32. O. Krauth, G. Fahsold, A. Pucci, Asymmetric line shapes and surface enhanced infrared absorption of CO adsorbed on thin Fe films on MgO(001), J. Chem. Phys. **110**, 3113–3117 (1999) 164, 171
33. A. Wakaun, Surface-enhanced electromagnetic processes, in *Solid State Physics*, H. Ehrenreich, D. Turnbull (Eds.) (Academic, New York, 1984) **38**, pp. 223–294 164, 165, 167
34. J. I. Gersten, A. Nitzan, Photophysics and photochemistry near surfaces and small particles, Surf. Sci. **158**, 165–189 (1985) 164, 165, 167
35. M. Osawa, K. Ataka, Electromagnetic mechanism of enhanced infrared absorption of molecules adsorbed on metal island films, Surf. Sci. Lett. **262**, L118–L122 (1992) 164, 170
36. B. N. J. Persson, R. Ryberg, Vibrational interaction between molecules adsorbed on a metal surface: the dipole–dipole interactions, Phys. Rev. B **24**, 6954–6970 (1981) 164, 171
37. B. N. J. Persson, A. Liebsch, Collective vibrational models of isotope mixture of CO on Cu(111) and Cu(001), Surf. Sci. **110**, 356–368 (1981) 164, 171
38. P. Dumas, R. G. Tobin, P. Richards, Study of adsorption states and interactions of CO on evaporated noble metal surfaces by infrared absorption spectroscopy. 1. Silver, Surf. Sci. **171**, 555–578 (1986) 164, 171
39. Y. Nishikawa, K. Fujiwara, T. Shima, Quantitative analysis of nanogram samples with Fourier transform infrared transmission surface electromagnetic wave spectroscopy, Appl. Spectrosc. **44**, 691–694 (1990) 164
40. S. A. Johnson, N.-H. Pham, V. J. Novick, V. A. Maroni, Application of surface-enhanced infrared absorption spectroscopy as a sensor for volatile organic compounds, Appl. Spectrosc. **51**, 1423–1426 (1997) 164

41. K. Ito, K. Hayashi, Y. Hamanaka, M. Yamamoto, T. Araki, K. Iriyama, Infrared and Raman scattering spectroscopic study on the structures of Langmuir–Blodgett monolayers contacting a merocyanine dye, Langmuir **8**, 140–147 (1992) 165
42. M. Osawa, N. Matsuda, K. Yoshii, I. Uchida, Charge transfer resonance Raman process in surface-enhanced Raman scattering from p-aminothiophenol adsorbed on silver: Herzberg-Teller contribution, J. Phys. Chem. **98**, 12702–12707 (1994) 165, 182
43. C. Kuhne, G. Steiner, W. B. Fischer, R. Salze, Surface-enhanced FTIR spectroscopy on membranes, Fresenius J. Anal. Chem. **360**, 750–754 (1998) 165, 167
44. R. Aroca, R. Bujalski, Surface-enhanced vibrational spectra of thymine, Vib. Spectrosc. **19**, 11–12 (1999) 165, 182
45. G. T. Merklin, L.-T. He, P. R. Griffiths, Surface-enhanced infrared absorption spectrometry of p-nitorothiophenol and its disulfide, Appl. Spectrosc. **53**, 1448–1453 (1999) 165
46. R. Kellner, B. Mizaikoff, M. Jakusch, H. D. Wanzenböck, N. Weissenbacher, Surface-enhanced vibrational spectroscopy: A new tool in chemical IR sensing?, Appl. Spectrosc. **51**, 495–503 (1997) 165
47. H. D. Wanzenböck, B. Mizaikoff, N. Weissenbacher, R. Kellner, Multiple internal reflection in surface enhanced infrared absorption spectroscopy (SEIRA) and its significance for various analyte groups, J. Mol. Struct. **410-411**, 535–538 (1997) 165
48. C. W. Brown, Y. Li, J. A. Seelenbinder, P. Pivarnik, A. G. Rand, S. V. Letcher, O. J. Gregory, and M. J. Platek, Immunoassays based on surface-enhanced infrared absorption spectroscopy, Anal. Chem. **70**, 2991–2996 (1998) 165
49. Y. Zhu, H. Uchida, M. Watanabe, Oxidation of carbon monoxide at a platinum film electrodes studied by Fourier transform infrared spectroscopy with attenuated total reflection technique, Langmuir **15**, 8757–8764 (1999) 165, 171, 174
50. M. Watanabe, Y. Zhu, H. Uchida, Oxidation of CO on a Pt–Fe alloy electrode studied by surface-enhanced infrared reflection-absorption spectroscopy, J. Phys. Chem. **104**, 1762–1768 (2000) 165, 171, 174
51. S. Sato, K. Kamada, M. Osawa, Surface-enhanced IR absorption (SEIRA) on small Pt particles deposited on an island Au film, Chem. Lett., 15–16 (1999) 165
52. Y. Nishikawa, K. Fujiwara, M. Osawa, K. Takamura, Trace analysis of human skin secretions by surface-enhanced infrared spectroscopy: Detection of Lactate, Anal. Sci. **9**, 811–815 (1993) 165
53. Y. Nishikawa, K. Fujiwara, K. Takamura, Trace analysis of residual additives on the surface of cultivated fruits by surface-enhanced infrared spectroscopy, Bunseki Kagaku **43**, 425–429 (1994) 165
54. M. Osawa, K. Yoshii, K. Ataka, T. Yotsuyanagi, Real-time monitoring of electrochemical dynamics by submillisecond time-resolved surface-enhanced infrared attenuated-total-reflection spectroscopy, Langmuir **10**, 640–642 (1994) 165, 177
55. M. Osawa, K. Yoshii, Y. Hibino, T. Nakano, I. Noda, Two-dimensional infrared correlation analysis of electrochemical reactions, J. Electroanal. Chem. **426**, 11–16 (1997) 165, 177

56. H. Noda, K. Ataka, L.-J. Wan, M. Osawa, Time-resolved surface-enhanced infrared study of molecular adsorption at the electrochemical interface, Surf. Sci. **427–428**, 190-194 (1999) 165, 174, 177, 179
57. K. Ataka, Y. Hara, M. Osawa, A new approach to electrode kinetics and dynamics by potential–modulated Fourier transform infrared spectroscopy, J. Electroanal. Chem. **473**, 34–42 (1999) 165, 174, 179, 180
58. K. Ataka, G. Nishina, W.-B. Cai, S.-G. Sun, M. Osawa, Dynamics of the dissolution of an underpotentially deposited Cu layer on Au(111): A combined time-resolved surface-enhanced infrared and chronocoulometric study, Electrochem. Commun. **2**, 417-421 (2000) 165, 174, 177
59. S. Yoshida, T. Yamaguchi, A. Kimbara, Optical properties of aggregated silver films, J. Opt. Soc. Am. **61**, 62 (1971) 166
60. W. N. Hansen, J. Opt. Soc. Am. **58**, 380 (1968) 167, 168
61. P. N. Sanda, J. E. Demuth, J. C. Tsang, J. M. Warlaumont, Coverage dependence, in *Surface Enhanced Raman Scattering*, R. K. Chang, T. E. Furtak (Eds.) (Plenum, New York 1982), pp. 189–221 167
62. A. Röseler, E.-H. Korte, The optical constant of metallic island films as used for surface enhanced infrared absorption, Thin Solid Films **313-314**, 732–736 (1998) 167
63. G. A. Niklasson, C. G. Granqvist, Optical properties and solar selectivity of coevaporated Co–Al2O3 composite films, J. Appl. Phys. **55**, 3382–3410 (1984) 168
64. B. A. Maxwell–Garnett, Philos. Trans. Royal. Soc. A **203**, 385–420 (1904) 168
65. D. A. G. Bruggemann, Berechnung verschiedener physikalischer Konstanten von heterogenen Substanzen, Ann. Phys. (Leipzig) **24**, 636–664 (1935) 168, 169
66. C. F. Eagen, Nature of the enhanced optical absorption of dye-coated Ag island films, Appl. Opt. **20**, 3035–3042 (1981) 168
67. E. C. Stoner, The demagneitizing factors for ellipsoids, Philos. Mag. **7**, 803–820 (1945) 168
68. T. Yamaguchi, S. Yoshida, A. Kimbara, Continuous ellipsometric determination of optical constants and thickness of a silver film during deposition, Jpn. J. Appl. Phys. **8**, 559–567 (1969) 169
69. M. R. Johnson, W. W. Christy, Optical constants of the noble metals, Phys. Rev. B **6**, 4370 (1972) 169
70. M. Osawa, K. Ataka, K. Yoshii, T. Yotsuyanagi, Surface-enhanced infrared ATR spectroscopy for in situ studies of electrode/electrolyte interfaces, J. Electron Spectrosc. Relat. Phenom. **64/65**, 371–379 (1993) 170, 171, 173
71. M. Osawa, K. Ataka, M. Ikeda, H. Uchihara, R. Nanba, Surface-enhanced infrared absorption spectroscopy: Mechanism and application to trace analysis, Anal. Sci. **7** (Suppl.), 503–506 (1991) 171
72. R. Aroca, B. Price, A New Surface for surface-enhanced infrared spectroscopy: Tin island films, J. Phys. Chem. B **101**, 6537–6540 (1997) 171, 182
73. T. Yoshidome, T. Inoue, S. Kamata, Intensity enhancement of the infrared transmission spectra of p-nitrobenzoic acid by the presence of the Pb films, Chem. Lett. **6**, 533–534 (1997) 171
74. J. P. Devlin, K. Consani, Metal surface spectroscopy, Charge transfer and totally symmetric mode activity, J. Phys. Chem. **85**, 2597–2598 (1981) 171

75. T. Wadayama, T. Sakurai, S. Ichikawa, W. Suëtaka, Charge-transfer enhancement in the infrared absorption of thiocyanate ions adsorbed on a gold electrode in the Kretschmann configuration, Surf. Sci. **198**, L359–L364 (1988) 171
76. T. Wadayama, Y. Momota, A. Hatta, W. Suëtaka, Polarization modulation IR spectroscopic study of electrochemically generated species from TCNQ at a gold electrode in the Kretschmann ATR geometry, J. Electroanal. Chem. **289**, 29–36 (1990) 171
77. R. J. Nichols, IR spectroscopy of molecules at the solid–solution interface, in Adsorption of molecules at metal electrodes, J. Lipkowski, P. N. Ross (Eds.) (VCH, New York 1992) Chap. 7 172, 173, 180
78. K. P. Ishida, P. R. Griffiths, Theoretical and experimental investigation of internal reflection at thin copper films exposed to aqueous solutions, Anal. Chem. **66**, 522-530 (1994) 173
79. K. Ataka, T. Yotsuyanagi, M. Osawa, Potential–dependent reorientation of water molecules at an electrode/electrolyte interface studied by surface-enhanced infrared absorption spectroscopy, J. Phys. Chem. **100**, 10664–10672 (1996) 173, 175
80. S.-G. Sun, W.-B. Cai, L.-J. Wan, M. Osawa, Infrared absorption enhancement for CO adsorbed on Au films in perchloric acid solutions and effects of surface structure studied by cyclic voltammetry, scanning tunneling microscopy, and surface-enhanced IR spectroscopy, J. Phys. Chem. **103**, 2460–2466 (1999) 174
81. K. Ataka, M. Osawa, In situ infrared study of water–sulfate coadsorption on gold(111) in sulfuric acid solution, Langmuir **14**, 951–959 (1998) 174, 175, 177
82. K. Ataka, M. Osawa, In situ infrared study of cytosine adsorption on gold electrodes, J. Electroanal. Chem. **460**, 188–196 (1999) 174, 177
83. I. Taniguchi, S. Yoshimoto, Y. Sunatani, K. Nishiyama, Potential and pH dependencies of adsorbed species of 2,4–pyridinethiol and 2–pyrimidinethiol on Au(111) electrode, Electrochem. **67**, 1197–1199 (1999) 174, 182
84. M. Hoon–Khosla, W. R. Fawcett, A. Chen, J. Lipkowski, B. Pettinger, A SNIFTIR study of the adsorption of pyridine at the Au(111) electrode–solution interface, Electrochim. Acta **45**, 611–621 (1999) 174, 175
85. L. Stolberg, S. Morin, J. Lipkowski, D. E. Irish, Adsorption of pyridine at the Au(111)–solution interface, J. Electroanal. Chem. **307**, 241–262 (1991) 176
86. Z. Q. Feng, T. Sagara, K. Niki, Application of potential-modulated UV–visible reflectance spectroscopy to electron transfer rate measurements for adsorbed species on electrode surfaces, Anal. Chem. **67**, 3564–3570 (1995) 179
87. J.-N. Chazalviel, V. M. Dubin, K. C. Mandel, F. Ozanam, Modulated infrared spectroscopy at the electrochemical interface, Appl. Spectrosc. **64/65**, 1411–1416 (1993) 180
88. C. M. Pharr, P. R. Griffiths, Step–scan FT–IR spectroelectrochemical analysis of surface and solution species in the ferricyanide/ferocyanide redox couple, Anal. Chem. **69**, 4665–4672 (1997) 180
89. L.-J. Wan, H. Noda, Y. Hara, M. Osawa, Effect of solution pH of a 4–mercaptopyridine monolayer self–assembled on Au(111), J. Electroanal. Chem. (2000) (in press) 182